Particle control in long-pulse discharge using divertor pumping in LHD

PAPER • OPEN ACCESS

Particle control in long-pulse discharge using divertor pumping in LHD

View the article online for updates and enhancements.

Physica Scripta

Particle control in long-pulse discharge using divertor pumping in LHD

G Motojima[1,2,*] , S Masuzaki[1,2] , T Morisaki[1,2] , K Y Watanabe[1], M Kobayashi[1,2] , K Ida[1,2] ,
R Sakamoto[1,2] , M Yoshinuma[1], R Seki[1,2], H Nuga[1], T Tsujimura[1] , C Suzuki[1] , M Emoto[1],
Y Tsuchibushi[1], T Murase[1] and Y Takeiri[1,2]

[1]   National Institute for Fusion Science, National Institutes of Natural Sciences, 322-6 Oroshi-cho, Toki, Gifu 509-5292, Japan
[2]   SOKENDAI (The Graduate University for Advanced Studies), 322-6 Oroshi-cho, Toki, Gifu 509-5292, Japan
*   Author to whom any correspondence should be addressed.

E-mail: motojima.gen@nifs.ac.jp

Abstract

Density control is crucial for maintaining stable confined plasma. Divertor pumping, where neutral particles are compressed and exhausted in the divertor region, was developed for this task for the Large Helical Device. In this study, neutral particle pressure, which is related to recycling, was systematically scanned in the magnetic configuration by changing the magnetic axis position. High neutral particle pressure and compression were obtained in the divertor for a high plasma electron density and the inner magnetic axis configuration. Density control using divertor pumping with gas puffing was applied to electron cyclotron heated plasma in the inner magnetic axis configuration, which provides high neutral particle compression and exhaust in the divertor. Stable plasma density and electron temperature were maintained with divertor pumping. A heat analysis shows that divertor pumping did not affect edge electron heat conductivity, but it led to low electron heat conductivity in the core caused by electron-internal-transport-barrier-like formation.

1. Introduction

Density control is critical in fusion devices for maintaining high-performance plasma. Divertor pumping, where neutral particles are compressed and exhausted efficiently with a baffle structure [1], was developed for this task. Density control is challenging for long-pulse discharge because wall recycling changes with time [2–5]. For example, in the Large Helical Device (LHD) [6], one of the largest superconducting helical/stellarator fusion devices, dynamic wall retention was observed in 48 min of long-pulse discharge [7]. Basic density control via gas puffing is thus insufficient. In tokamaks such as JT-60U, density feedback in the latter phase of discharge was not well controlled by wall saturation in 40 s ELMy H-mode discharge [8]. Wall recycling is related to neutral particles [9, 10]. Therefore, neutral particle control is required in fusion devices for density control.

Neutral particle compression in a divertor with baffle structures has been obtained in various devices. For the LHD, the development of divertor pumping on the inboard side of the divertor region started in 2012. In the first phase of development, the topological structure of the divertor was changed from an open structure to a closed structure. The modified divertor tiles are facing to the private region not to the plasmas. This increased the neutral particle compression in the closed divertor by a factor of 10 [11]. A cryo-sorption pump [12] and a non-evaporable getter pump [13] were then installed for exhausting the compressed neutral particles. As a result, the divertor pumping achieved a low recycling state [14]. In the TCV tokamak, a significant increase (by a factor of 2–5) in divertor neutral particle pressure was recently obtained with baffles [15]. High neutral particle pressure in the divertor is key for controlling access to detachment in the ASDEX-Upgrade [16]. SOLPS-ITER simulation showed that divertor pumping has a significant effect on detachment onset [17]. Thus, neutral particle compression in the divertor is an important factor for plasma control. An in-vessel cryopump was designed for

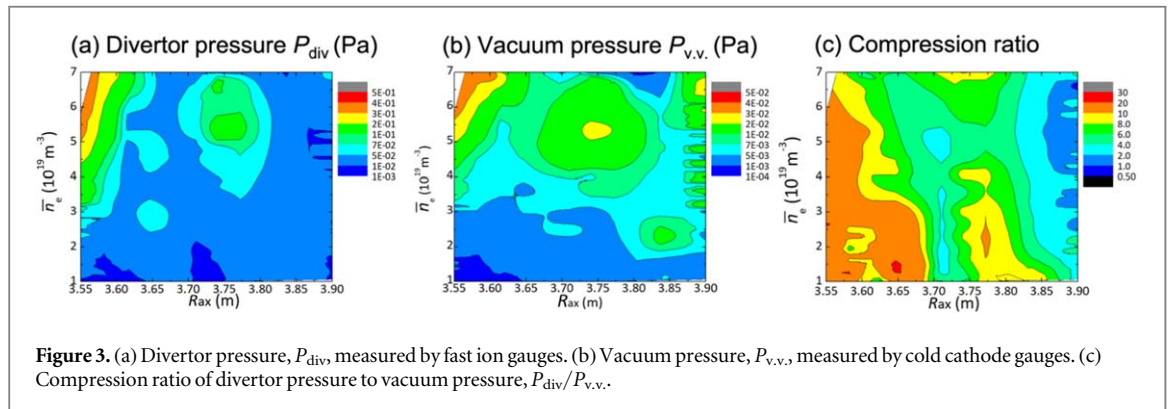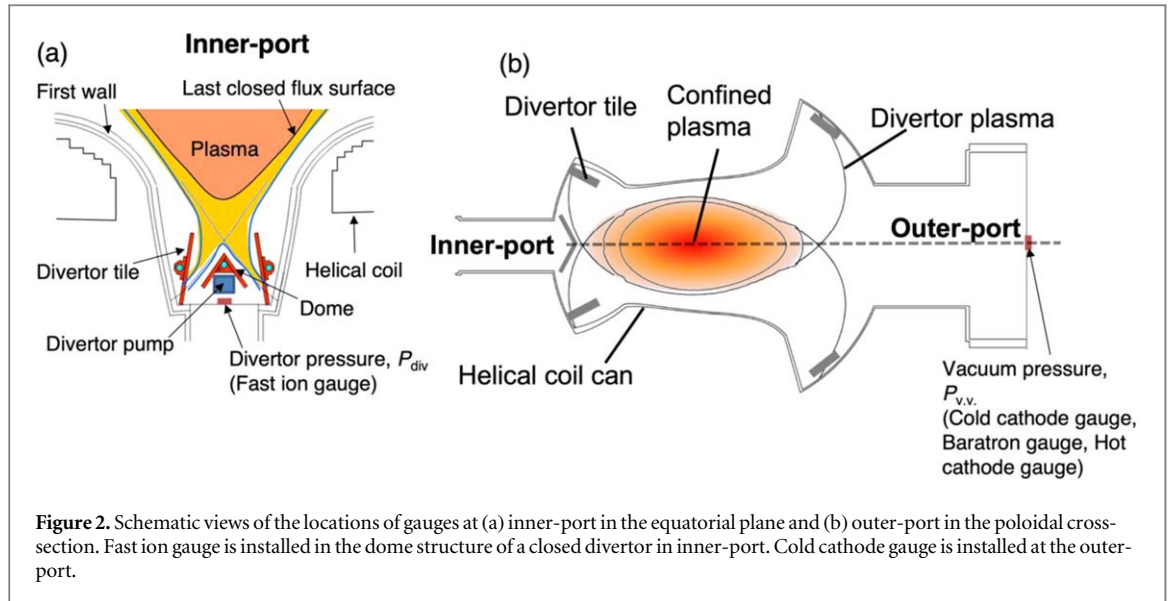**Figure 1.** Neutral particle pressure diagnostics in LHD.
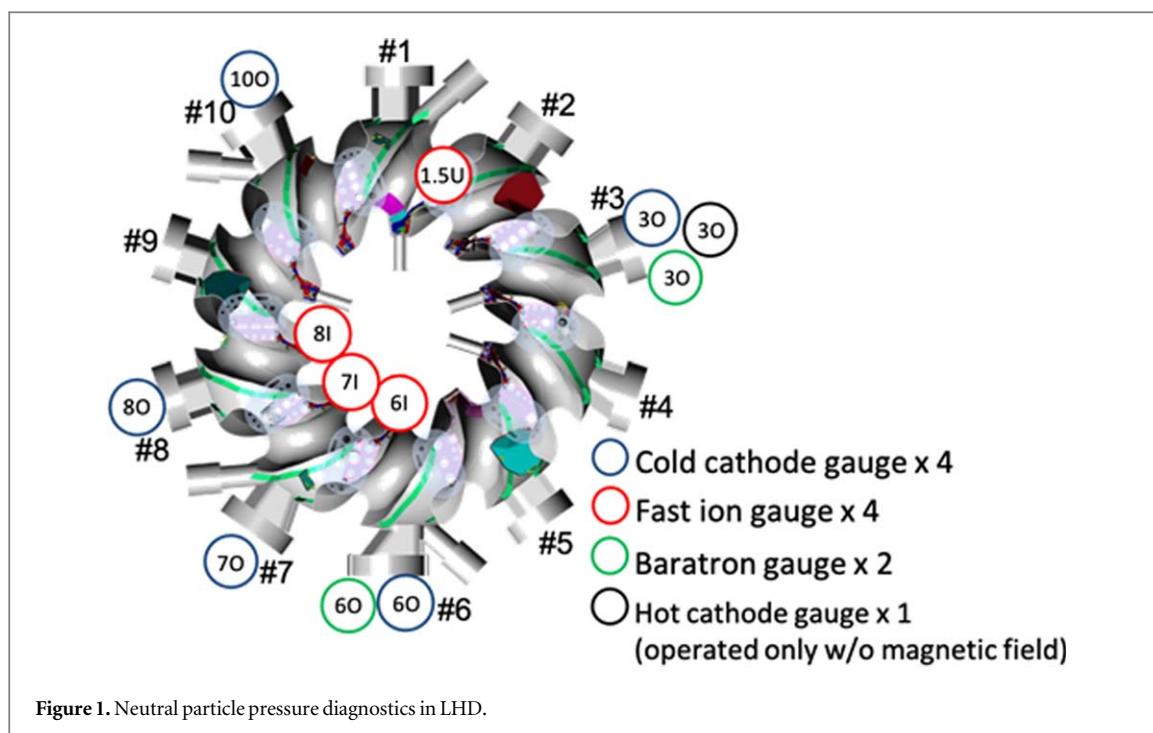
the new upper divertor in the ASDEX Upgrade [18] and a cryo-sorption pump was designed for divertor pumping for ITER [19].

This study presents the experimental results of divertor pumping applied for 40 s to electron cyclotron heated (ECH) plasma. The rest of this paper is organized as follows. In section 2, neutral particle pressure measurements by fast ion gauges are described. In section 3, the dependence of neutral particle pressure on the magnetic configuration is systematically investigated. The experimental results with divertor pumping for 40 s of ECH plasma are also described. In section 4, the discussion of the difference of plasma performance with and without divertor pumping is discussed. In section 5, conclusions are given.

2. Neutral particle measurement by fast ion gauges

Neutral particle pressure can be measured using various vacuum pressure gauges. In an environment with a magnetic field, fast ion gauges are utilized [20]. The mechanism of these gauges can be briefly explained as follows. The electrons emitted from a filament heated by an electric current of about 16–19 A are accelerated by the potential gradient between the acceleration grid and the filament. The ions produced by the ionization of neutral gas are collected by an ion collector. The electron flux from the filament to the acceleration grid is chopped by sweeping the control grid potential at high frequency, during which the offset due to the background plasma (if any) is measured. The offset is subtracted from the ion collector current to obtain the net ion current from only the neutral particles. The ion current depends on neutral particle pressure, and thus the measured ion current reflects the neutral particle pressure. Thoriated tungsten is conventionally utilized for the filament. However, LaB_6, which can reduce the filament current, is utilized for collaboration research [21].

Figure 1 shows the locations of gauges in the LHD. Four fast ion gauges are installed. Three of them are in the divertor on the inboard side (6I, 7I, and 8I) and the other is on the port at the top (1.5U). Here, the number represents the section where the gauge was installed (the LHD has 10 toroidal sections). Four cold cathode gauges (3O, 6O, 8O, and 10O) and two baratron gauges (3O and 6O) are installed in the outer port of the torus. One hot cathode gauge (3O) is installed; it is operated only when there is no magnetic field. The divertor pressure is a neutral pressure in the closed divertor measured by the fast ion gauges and the vacuum pressure is a neutral pressure at an outer port measured by the cold cathode gauges. Figure 2 shows the schematic view of the locations of the gauges. The divertor pressure measures the neutral particles compressed by the closed divertor as shown in figure 2(a) which shows the location in the equatorial plane. On the other hand, the vacuum pressure measures the neutral particles at the outer ports as shown in figure 2(b) which shows the location in the poloidal cross-section.
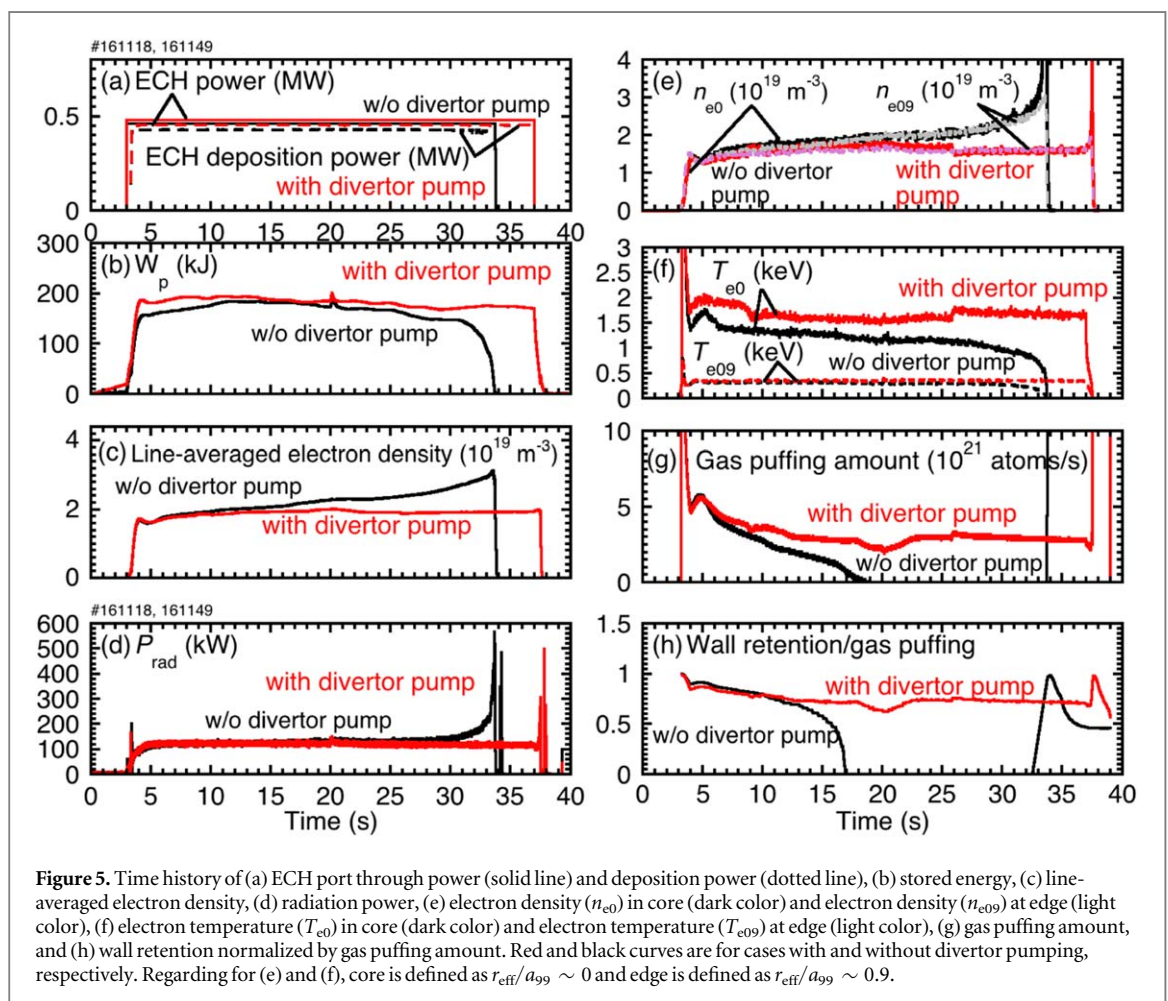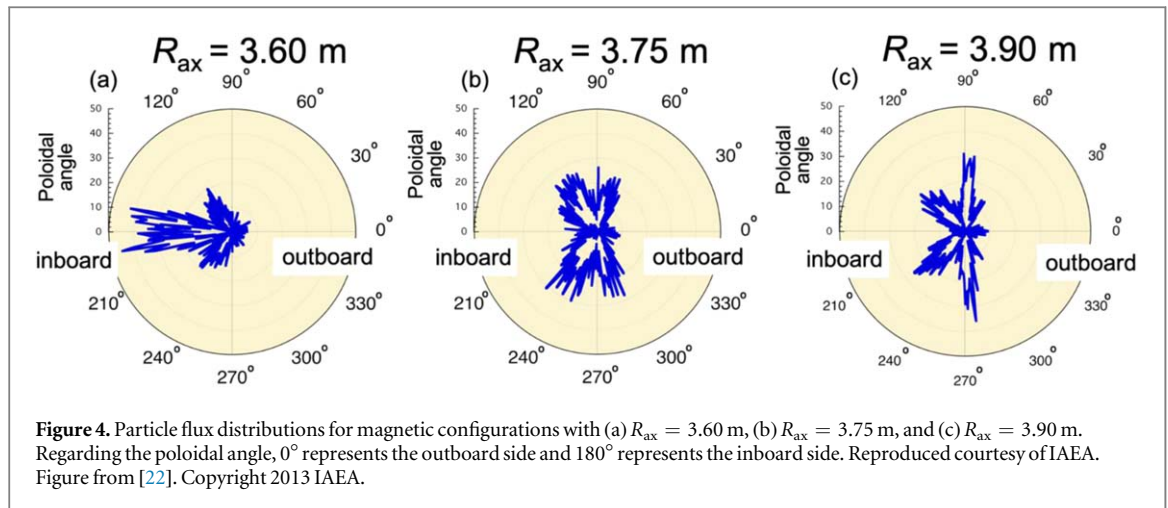
Figure 2. Schematic views of the locations of gauges at (a) inner-port in the equatorial plane and (b) outer-port in the poloidal cross-section. Fast ion gauge is installed in the dome structure of a closed divertor in inner-port. Cold cathode gauge is installed at the outer-port.

Figure 3. (a) Divertor pressure, P_{div}, measured by fast ion gauges. (b) Vacuum pressure, $P_{\text{v.v.}}$, measured by cold cathode gauges. (c) Compression ratio of divertor pressure to vacuum pressure, $P_{\text{div}}/P_{\text{v.v.}}$.

3. Experimental Results

3.1. Dependence of neutral particles on magnetic configuration

LHD has a flexibility of the experimental magnetic configuration by shifting the major radius of the magnetic axis (R_{ax}). We systematically investigated the neutral particle dependence on plasma electron density and magnetic configuration. Figures 3(a)–(c) respectively shows contour plots of the neutral particle pressure in the divertor (P_{div}), the vacuum pressure ($P_{\text{v.v.}}$), and the compression ratio of the divertor pressure to the vacuum pressure ($P_{\text{div}}/P_{\text{v.v.}}$) in terms of average electron density ($\bar{n}_e$) versus magnetic configurations shown by R_{ax}. Both P_{div} and $P_{\text{v.v.}}$ are higher for the inner R_{ax} magnetic configuration. The tendency is clearer in the high-n_e regime. Both P_{div} and $P_{\text{v.v.}}$ tend to increase with electron density, especially for the inner R_{ax} magnetic configuration, due to high particle fluxes in the divertor. A comparison of figures 3(a) and (b) indicates that P_{div} is 10 times higher than $P_{\text{v.v.}}$. Neutral particle compression, $P_{\text{div}}/P_{\text{v.v.}}$, is 10–20 in configurations with $R_{\text{ax}} < 3.7$ m. Thus, the inner R_{ax} configuration is most suitable for obtaining higher neutral particle pressure and compression.

The reason for the higher neutral particle pressure for the inner R_{ax} magnetic configuration is discussed below. Figure 4 shows the particle flux distribution in the poloidal plane for three R_{ax} configurations ($R_{\text{ax}} = 3.60, 3.75,$ and 3.90 m). Here, 0° and 180° represent the divertor on the outboard and inboard sides, respectively. For the $R_{\text{ax}} = 3.60$ m configuration, the particle flux distribution is localized on the inboard side. 90% of the particles are localized on inboard side for this configuration. In contrast, for $R_{\text{ax}} = 3.75$ and 3.90 m, the particle flux is widely distributed. Only 60% of the particles are localized on the inboard side for the $R_{\text{ax}} = 3.90$ m configuration. For the inner R_{ax} magnetic configuration, the particle flux is efficiently localized on the inboard side of the divertor. The inner R_{ax} magnetic configuration is most suitable for particle exhaust by divertor pumping because the closed divertor system with exhaust pumps was developed on the inboard side of the torus.

Figure 4. Particle flux distributions for magnetic configurations with (a) $R_{ax} = 3.60$ m, (b) $R_{ax} = 3.75$ m, and (c) $R_{ax} = 3.90$ m. Regarding the poloidal angle, 0° represents the outboard side and 180° represents the inboard side. Reproduced courtesy of IAEA. Figure from [22]. Copyright 2013 IAEA.

Figure 5. Time history of (a) ECH port through power (solid line) and deposition power (dotted line), (b) stored energy, (c) line-averaged electron density, (d) radiation power, (e) electron density (n_{e0}) in core (dark color) and electron density (n_{e09}) at edge (light color), (f) electron temperature (T_{e0}) in core (dark color) and electron temperature (T_{e09}) at edge (light color), (g) gas puffing amount, and (h) wall retention normalized by gas puffing amount. Red and black curves are for cases with and without divertor pumping, respectively. Regarding for (e) and (f), core is defined as $r_{eff}/a_{99} \sim 0$ and edge is defined as $r_{eff}/a_{99} \sim 0.9$.

3.2. Long-pulse discharge using divertor pump

To investigate the effect of divertor pumping on density control, divertor pumping was applied for 40 s to ECH plasma discharges. The pumping speed of the divertor was 70 m^3 s^{-1} for hydrogen gas. The density was maintained by feedback control of the signal of line-averaged electron density. The magnetic configuration was $R_{ax} = 3.60$ m for efficient neutral particle compression, as discussed above. Figure 5 shows the time history of the results obtained with and without divertor pumping. As shown in figure 5(a), similar ECH port through power was utilized. Figures 5(b), (c), and (g) shows that without divertor pumping, even without gas puffing, the plasma electron density gradually increased and the density was not well controlled by density feedback. Plasma radiation eventually collapsed, decreasing the stored energy during the electron cyclotron heating. We confirmed that the diamagnetic kinetic energy obtained from the profiles is consistent with the plasma stored
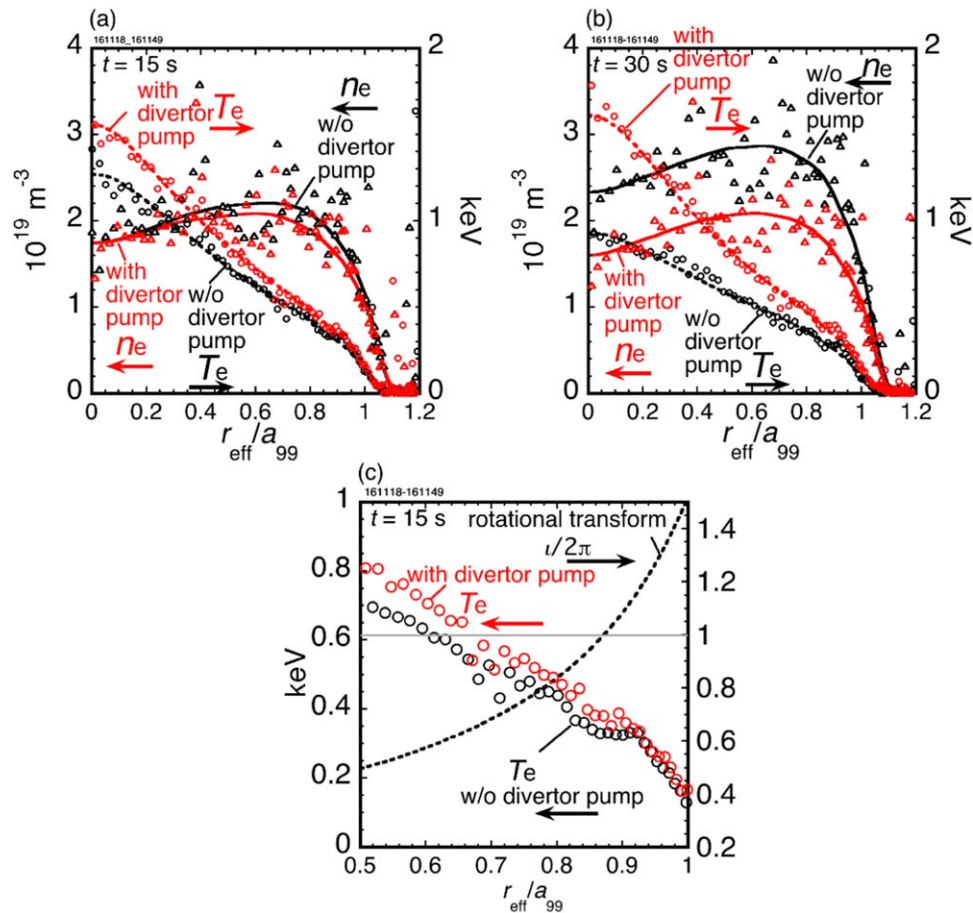
Figure 6. Electron density (n_e) and temperature (T_e) profiles with and without divertor pumping at (a) $t = 15$ s and (b) $t = 30$ s. Lines show polynomial fit to data. The extended temperature profiles at $t = 15$ s are shown in (c). Dotted line represents the rotational transform, $\iota/2\pi$. Red and black results are for the cases with and without divertor pumping, respectively.

energy (within 10%). As shown in figure 5(d), radiation power was similar in both cases. The central electron temperature decreased whereas central electron density increased with time for the case without divertor pumping (see figures 5(e) and (f)). With divertor pumping, density feedback control was well operated by stable gas puffing of hydrogen. The central electron temperature and central electron density were maintained. A particle balance analysis shows that the exhausted amount for the case with divertor pumping was up to 50 times larger than that for the case without divertor pumping. Figure 5(h) shows the wall retention amount normalized by the gas puffing amount. Without divertor pumping, wall retention was rapidly reduced at $t \sim 17$ s, indicating clear wall saturation. In contrast, with divertor pumping, wall recycling continued until the end of the discharge. The results indicate that efficient particle control can be achieved using divertor pumping without wall saturation.

Figure 6(a) shows the bulk electron density and temperature profiles in the first phase of discharge ($t = 15$ s) with and without divertor pumping for 40 s of ECH plasma discharges. In the first phase of discharge, the electron density profiles are similar; they are slightly higher especially in $0.5 < r_{eff}/a_{99} < 0.9$ for the case without divertor pumping. Here, r_{eff} is the radius of the equivalent simple torus enclosing the same volume as that enclosed by the flux surface of interest and a_{99} is the effective minor radius that encloses 99% of the total electron pressure. The hollow level of the profile is higher without divertor pumping. In contrast, the temperature profiles show a clear difference. A higher central temperature is obtained with divertor pumping. The difference is due to the temperature flattening by the magnetic island at $r_{eff}/a_{99} \sim 0.8$–0.9. Figure 6(c) shows the extended temperature profiles at the edge along with the rotation transform ($\iota/2\pi$ profile. Around $r_{eff}/a_{99} \sim 0.8$–0.9, a flattening of the temperature, which corresponds to the rotational transform $\iota/2\pi = 1$, is observed for the case without divertor pumping. The flattening probably resulted from the difference in electron density at the edge. Without divertor pumping, the density at $r_{eff}/a_{99} \sim 0.8$–0.9 is higher than that with divertor pumping. The higher density might change the flattening width of the island. The different neutral particle profile might also change the plasma rotation frequency, presumably affecting magnetic island formation. To verify these assumptions, further measurements of plasma flow and neutral particle profiles are required. Such
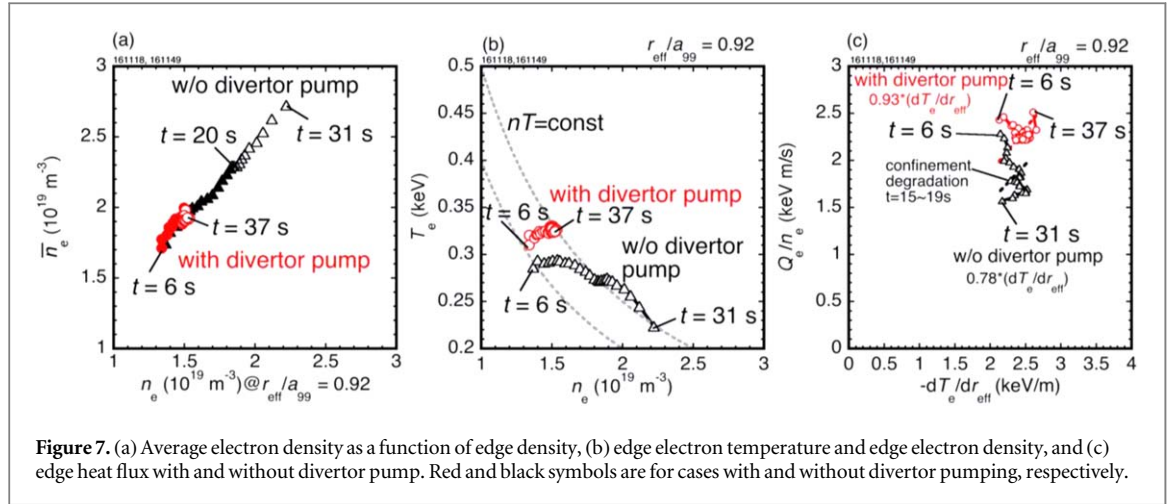
Figure 7. (a) Average electron density as a function of edge density, (b) edge electron temperature and edge electron density, and (c) edge heat flux with and without divertor pump. Red and black symbols are for cases with and without divertor pumping, respectively.

measurements will be conducted in near future. Figure 6(b) shows the electron density and temperature profiles in the end phase of discharge ($t = 30$ s) with and without divertor pumping for 40 s of ECH plasma discharges. In the end phase of discharge, both the electron density and temperature profiles are different for the cases with and without divertor pumping. The density along the minor radius is higher without divertor pumping, whereas the temperature along the minor radius is higher with divertor pumping. In LHD, electron internal transport barrier (e-ITB) plasma with a large temperature gradient in the plasma core ($r_{eff}/a_{99} < 0.3$) was observed in ECH heating [23–25]. Such a large temperature gradient in the plasma core was not observed in the discharges reported in this study. However, a peaked temperature profile with a critical point of temperature gradient at $r_{eff}/a_{99} \sim 0.4$ was obtained in the discharge with divertor pumping. In this study, the temperature profile is called as e-ITB like profile. The temperature profile was not changed in time in the case with divertor pumping.

The time history of density and temperature in the edge region is discussed. Figure 7(a) shows the relation between the average electron density and edge density. The edge density was set to $r_{eff}/a_{99} = 0.92$. Both with and without divertor pumping, the average n_e linearly increased with edge n_e. This indicates that the edge density is a key factor for controlling the average n_e. Figure 7(b) shows the relation between the edge electron temperature and the edge n_e. Here, the edge temperature was also set to $r_{eff}/a_{99} = 0.92$. Without divertor pumping, the density increases and the temperature decreases. In contrast, with divertor pumping, a stable edge density and temperature are maintained. The difference of the density between with and without divertor pumping is due to the fuel particle source. In the case with divertor pumping, the fueling source was gas puffing. On the other hand, in the case without divertor pumping, the fueling source was changed from gas puffing to wall recycling as shown in figure 5(h). In the phase of wall recycling, the electron density control was not possible, resulting that the density was increased compared with that with divertor pumping. The dotted lines, which represent constant $n_e T_e$, show that for both cases, the edge pressure increases with time. This characteristic is different from that reported for JT-60U, for which the edge pressure decreased [8]. The plasma current might be responsible for this difference. In tokamaks, the electron density is limited by the plasma current (Greenwald density limit) [26]. A higher density makes the operating space narrow for the required plasma current. As a result, a lower plasma current triggers the confinement limit. In contrast, in the LHD, operation at densities over the Greenwald limit is possible [27]. This is because no plasma current is required for confinement in stellarator/helical devices. Therefore, the difference in the edge pressure dependence on time between the LHD and JT-60U might be attributed to the plasma current in the wall saturation phase.

Figure 7(c) shows the results of an edge heat flux analysis. We developed a module called dytrans_ts for analyzing the heat flux and heat conductivity of ions and electrons. dytrans_ts is available in AutoAna [28], a tool that automatically calculates the physical data for the LHD server. This module is starting to be utilized for transport analysis [29]. In the analysis, ECH power deposition (P_{ECH}) profiles calculated using the ray-tracing code LHDGauss [30] and neutral beam injection (NBI) deposition power profiles that consider slowdown calculated using CONV_FIT3D code [31] are utilized. In this study, only electron cyclotron heating is utilized; NBI deposition power profiles are not taken into account because of the lack of NBI heating (the ion heat flux, Q_i, is zero). The electron/ion temperature and density profiles mapped as a function can be found in Ref. [32]. Figure 7(c) shows the electron heat flux (Q_e) normalized by the electron density as a function of the T_e gradient in the edge region of $r_{eff}/a_{99} = 0.92$. Without divertor pumping, the normalized electron heat flux decreases with time due to the increase in electron density. In contrast, with divertor pumping, the normalized electron heat flux is maintained during the whole plasma discharge. The gradient of Q_e/n_e to $-dT_e/dr_{eff}$ evaluated over the whole discharge time is 0.93 and 0.78 with and without divertor pumping, respectively. Therefore, there is no
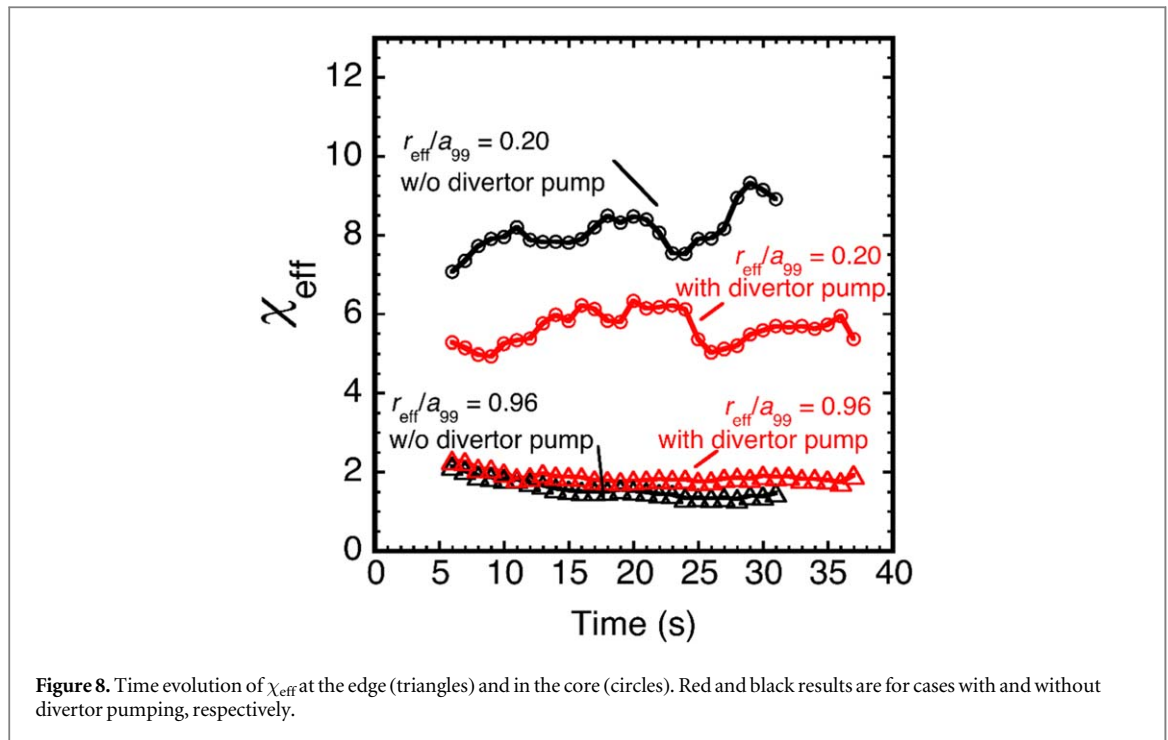
Figure 8. Time evolution of χ_{eff} at the edge (triangles) and in the core (circles). Red and black results are for cases with and without divertor pumping, respectively.

significant difference in the gradient in the plasma edge region. The analysis of heat conductivity of electrons, χ_{eff}, at the plasma edge shows the same characteristics, where χ_{eff} is defined as $\chi_{\mathrm{eff}} = (Q_e + Q_i)/(n_e \, \mathrm{d}T_e/\mathrm{d}r_{\mathrm{eff}} + n_i \, \mathrm{d}T_i/\mathrm{d}r_{\mathrm{eff}})$ under the assumption that $n_e = n_i$, and $T_e = T_i$. In this analysis, the ion temperature (T_i) is not measured by charge exchange spectroscopy. Therefore, equipartition is not quantitatively evaluated and must be assumed. Figure 8 shows χ_{eff} in the plasma edge region ($r_{\mathrm{eff}}/a_{99} = 0.96$). χ_{eff} at the plasma edge is similar (less than 16% difference) for the cases with and without divertor pumping. Figure 8 also shows the heat conductivity of electrons in the core ($r_{\mathrm{eff}}/a_{99} = 0.20$). In the core region with divertor pumping, low χ_{eff} is maintained for the whole plasma discharge. This is probably due to the e-ITB like formation. The direct effect of divertor pumping on plasma core performance is not fully understood; it will thus be further investigated in the future. A high ion temperature plasma with ion internal transport barriers has been achieved by reducing wall recycling in the LHD [33]. These results suggest that neutral particle control is a key factor for high-performance plasma.

4. Discussion

In this section, it will be discussed about the reasons why the plasma with divertor pumping related to this paper lowers the electron heat conductivity at $r_{\mathrm{eff}}/a_{99} = 0.20$ comparing with the plasma without divertor pumping, although the reproducibility is considered as a part of important future work.

Firstly, the difference of electron density in the cases with and without divertor pumping is discussed. The experimental results show that the line-averaged electron density, $\bar{n}_e$, is higher in the case without divertor pumping due to the lack of the density feedback control. In the first half of the discharge $t = 15$ s as shown in figure 5(c), the difference of line-averaged electron density seems small. However, in the density profile especially in $0.5 < r_{\mathrm{eff}}/a_{99} < 0.9$, the electron density was smaller in the case with the divertor pumping as shown in figure 6(a). Thus, it is possible that the decrease in the electron density causes the increase of the electron temperature in ECH heated plasmas.

Secondly, the difference of deposition power of ECH between with and without divertor pumping is discussed. Comparing the ECH deposition power, P_{dep}, in the cases with and without divertor pumping, the ECH deposition power in the case with divertor pumping is approximately 6% higher (0.45 ± 0.02 MW in the case with divertor pumping and 0.42 ± 0.02 MW in the case with divertor pumping). It is possible that the difference of deposition power contributes to the electron temperature increase.

The difference of electron temperature in the plasma core in the cases with and without divertor pumping may be discussed in the relation to the threshold of $P_{\mathrm{dep}}/\bar{n}_e$ for e-ITB like gradient formation in radial profile of electron temperature. Figure 9 shows the time evolution of ECH deposition power normalized by line-averaged electron density, $P_{\mathrm{dep}}/\bar{n}_e$, which is the parameter discussed in Ref. [23–25] related to the threshold condition
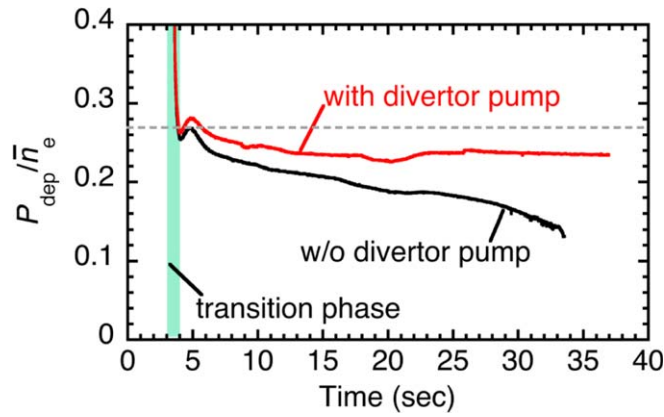
Figure 9. Time evolution of ECH deposition power normalized by line-averaged electron density. Red and black results are for cases with and without divertor pumping, respectively. Dotted line represents the maximum value attained at $t = 5$ s in the case without divertor pumping.
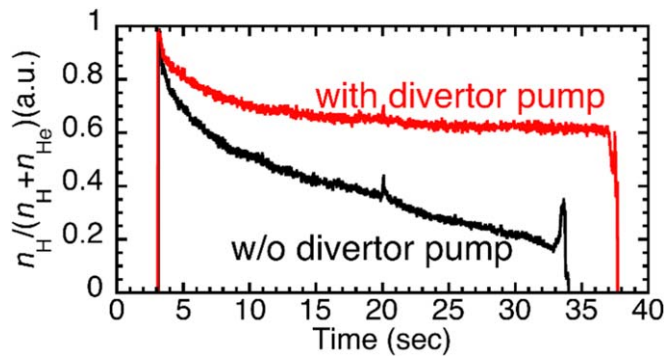

Figure 10. Time evolution of the concentration ratio of $n_H/(n_H + n_{He})$. Red and black results are for cases with and without divertor pumping, respectively.

for the ITB formation. As shown in figure 5(f), the core electron temperature appears to be higher in the case without divertor pumping at $t = 5$ s, with an e-ITB-like gradient similar to that with divertor pumping. After that, the density increases and $P_{dep}/\bar{n}_e$ decreases. From this result, it can be considered as follows in the case of without divertor pumping: $P_{dep}/\bar{n}_e$ reaches its maximum at $t = 5$ s, but the transition is not complete and $P_{dep}/\bar{n}_e$ starts to decrease, resulting into the non-transition state. On the other hand, in the case with divertor pumping, the $P_{dep}/\bar{n}_e$ is sufficiently large to make the transition to e-ITB like formation. Once the transition is attained, it continues to maintain the e-ITB like formation even if $P_{dep}/\bar{n}_e$ decreases after $t = 5$ s for a hysteresis.

Thirdly, the difference of concentration ratio of $n_H/(n_H + n_{He})$ in the cases with and without divertor pumping is discussed. Here, n_H is H^+ ion density and n_{He} is He^{2+} ion density which are estimated from the intensities of the H_α (656.3 nm) and HeI (587.6 nm). The ratio was different in the discharges with and without divertor pumping due to the constraints of other experimental conditions with the use of helium gas puffing. Figure 10 shows the time history of the ratio in the cases with and without divertor pumping. The ratio was smaller in the case without divertor pumping, indicating that the helium fraction is higher in the case without divertor pumping, although the total radiation power remains unchanged in both cases as shown in figure 5(d). In LHD, heat and particle transport in hydrogen and helium plasmas were compared in ECH heating and the experimental results showed that electron heat transport is comparable in both plasmas [34, 35]. In the discharges related to this paper, the concentration ratio is different, but it is likely that the lower electron heat conductivity at $r_{eff}/a_{99} = 0.20$ in the case with divertor pumping is not due to the difference of the concentration ratio of hydrogen and helium ion densities.

Fourthly, the non-local transport is discussed. In LHD, the nonlocal rise of electron temperature is observed. For example, the rise of non-local electron temperature is observed in the plasma with an e-ITB with ECH heated plasmas [36]. Also, by tracer-encapsulated solid pellet (TESPEL) [37], the rise of core electron temperature is invoked by the rapid edge cooling [38]. Although, the theory of non-local transport phenomena

is still developed, the process is attempted to be explained in Ref. [39, 40]. A strong nonlinearity of the growth rate of the micro-scale turbulence can cause a ballistic front propagation of turbulence and gradient in radial direction. The turbulence and gradient are coupled in the distance much larger than the turbulence correlation length. The turbulence spreading can be a candidate for the non-locality phenomena. It is unclear whether the turbulence spreading is shown by the effect of divertor pumping, however it seems to be one possibility because edge density profiles are different between the cases with and without divertor pumping.

5. Conclusion

In this study, we investigated the dependence of neutral particle pressure, which is a key factor for controlling recycling, on the magnetic configuration in the LHD. The neutral particle pressures in the inner divertor and vacuum regions were systematically measured by fast ion gauges and cold cathode gauges. Higher neutral particle pressure and higher neutral particle compression were obtained in the high-density regimes due to the high particle flux, and in the inner R_{ax} magnetic configuration because the particle flux was focused on the inboard side of the divertor in this configuration. To control recycling, divertor pumping with the inner toroidal section enabling neutral particle compression and exhaust was utilized. Divertor pumping was applied for 40 s to ECH plasma discharge in the inner R_{ax} magnetic configuration. The electron density was well controlled by divertor pumping. A high T_e in the core was maintained with divertor pumping. A heat flux analysis showed that at the edge, the effective heat conductivity, χ_{eff}, is similar for the cases with and without divertor pumping. However, a high χ_{eff} in the core was obtained with divertor pumping because of e-ITB-like gradient formation of temperature profile.

Acknowledgments

Data availability statement

Data can be accessed from the Large Helical Device (LHD) data repository server of NationalInstitute for Fusion Science (NIFS) at https://www-lhd.nifs.ac.jp/pub/Repository_en.html.

ORCID iDs

G Motojima ● https://orcid.org/0000-0001-5522-3082
S Masuzaki ● https://orcid.org/0000-0003-0161-0938
M Kobayashi ● https://orcid.org/0000-0002-0990-7093
K Ida ● https://orcid.org/0000-0002-0585-4561
R Sakamoto ● https://orcid.org/0000-0002-4453-953X
T Tsujimura ● https://orcid.org/0000-0002-2983-5920
C Suzuki ● https://orcid.org/0000-0001-6536-9034

References

[1] Loarte A *et al* 2001 *Plasma Phys. Control. Fusion* **43** R183
[2] Sakamoto M *et al* 2002 *Nucl. Fusion* **42** 165
[3] Guo H Y *et al* 2014 *Nucl. Fusion* **54** 013002
[4] Schlisio G *et al* 2021 *Nucl. Fusion* **61** 036031
[5] Hanada K *et al* 2021 *Nucl. Mater. Energy* **27** 101013
[6] Komori A *et al* 2010 *Fusion Sci. Technol* **58** 1
[7] Motojima G *et al* 2015 *J. Nucl. Mater.* **463** 1080
[8] Kamada Y 2004 *Presented in Atomic Energy Society of Japan* (http://aesj.or.jp/~fusion/aesjfnt/H16-9kikaku-session/kamada.pdf) (in Japanese)
[9] Kobayashi S *et al* 1999 *J. Nucl. Mater.* **266-269** 566
[10] Lipschultz B *et al* 2002 *Plasma Phys. Control. Fusion* **44** 733
[11] Kawamura G *et al* 2014 *Contrib. Plasma Phys.* **54** 437
[12] Day C 2207 *CERN Accelerator School: Vacuum in Accelerators* (https://cds.cern.ch/record/1047069/files/p241.pdf) Proceedings
[13] Maccallini E *et al* 2012 *AIP Conf. Proc.* **1451** 24
[14] Motojima G *et al* 2019 *Nucl. Fusion* **59** 086022
[15] Fevrier O *et al* 2021 *Nucl. Mater. Energy* **27** 100977

[16] Kallenbach A *et al* 2015 *Nucl. Fusion* **55** 053026
[17] Sang C *et al* 2021 *Nucl. Fusion* **61** 016022
[18] Schall G *et al* 2021 *Fusion Eng. Des.* **166** 112316
[19] Pearce R *et al* 2013 *Fusion Eng. Des.* **88** 809
[20] Haas G *et al* 1998 *Vacuum* **51** 39–46
[21] Wenzel U *et al* 2018 *Rev. Sci. Instrum.* **89** 033503
[22] Morisaki T *et al* 2013 *Nucl. Fusion* **53** 063014
[23] Yokoyama M *et al* 2007 *Nucl. Fusion* **47** 1213
[24] Yoshimura Y *et al* 2018 *Plasma Phys. Control. Fusion* **60** 025012
[25] Takahashi H *et al* 2018 *Nucl. Fusion* **58** 106028
[26] Greenwald M *et al* 1988 *Nucl. Fusion* **28** 2199
[27] Yamada H 2010 *Fusion Sci. Technol.* **58** 12
[28] Emoto M *et al* 2018 *Fusion Sci. Technol.* **74** 161
[29] Nespoli F *et al* 2021 *Nature Physics.* (https://researchsquare.com/article/rs-614131/v1) early view (https://doi.org/10.21203/rs.3.rs-614131/v1)
[30] Ii Tsujimura T *et al* 2015 *Nucl. Fusion* **55** 123019
[31] Nuga H *et al* 2020 *J. Plasma Phys.* **86** 815860306
[32] Suzuki C *et al* 2013 *Plasma Phys. Control. Fusion* **55** 014016
[33] Nagaoka K *et al* 2015 *Nucl. Fusion* **55** 113020
[34] Tanaka K *et al* 2017 *Nucl. Fusion* **57** 116005
[35] Makino R *et al* 2014 *Heat and particle transport in hydrogen and helium ECH plasmas on LHD 41st European Physical Society Conf. on Plasma Physics (Berlin)* p P4.087 (http://ocs.ciemat.es/EPS2014PAP/pdf/P4.087.pdf)
[36] Shimozuma T *et al* 2003 *Plasma Phys. Control. Fusion* **45** 1183
[37] Sudo S *et al* 2012 *Nucl. Fusion* **52** 063012
[38] Tamura N *et al* 2007 *Nucl. Fusion* **47** 449
[39] Yi S *et al* 2015 *Nucl. Fusion* **55** 092002
[40] Ida K *et al* 2015 *Nucl. Fusion* **55** 013022